Unconditional preparation of nonclassical states via linear-and-quadratic optomechanics

Matteo Brunelli,[1] Oussama Houhou,[2,3] Darren W. Moore,[2,4] Andreas Nunnenkamp,[1]
Mauro Paternostro,[2] and Alessandro Ferraro[2]

[1]*Cavendish Laboratory, University of Cambridge, Cambridge CB3 0HE, United Kingdom*
[2]*Centre for Theoretical Atomic, Molecular, and Optical Physics, School of Mathematics and Physics, Queen's University, Belfast BT7 1NN, United Kingdom*
[3]*Laboratory of Physics of Experimental Techniques and Applications, University of Medea, Medea 26000, Algeria*
[4]*Department of Optics, Palacký University, 17. listopadu 1192/12, 771 46 Olomouc, Czech Republic*

(Received 9 April 2018; published 3 December 2018)

Reservoir engineering enables the robust and unconditional preparation of pure quantum states in noisy environments. We show how a family of nonclassical states of a mechanical oscillator can be stabilized in a cavity that is parametrically coupled to both the mechanical displacement and the displacement squared. The cavity is driven with three tones, on the red sideband, on the cavity resonance, and on the second blue sideband. The states so stabilized are (squeezed and displaced) superpositions of a finite number of phonons. They show the unique feature of encompassing two prototypes of nonclassicality for bosonic systems: by adjusting the strength of the drives, one can in fact move from a single-phonon- to a Schrödinger-cat-like state. The scheme is deterministic, supersedes the need for measurement-and-feedback loops, and does not require initialization of the oscillator to the ground state.

DOI: 10.1103/PhysRevA.98.063801

I. INTRODUCTION

The preparation and manipulation of pure quantum states usually requires isolation of the system from the surrounding environment and control of the Hamiltonian. Pursuing a radically different approach, reservoir engineering aims instead to stabilize genuine quantum features of a system by tailoring the properties of the environment [1]. Such a technique has proven particularly successful in cavity systems, where a damped cavity mode naturally provides a highly tunable reservoir. Reservoir engineering has been successfully applied to trapped atoms [2] and ions [3–5], circuit quantum electrodynamics [6,7] and opto- and electromechanics [8–12]. Focusing on cavity optomechanics, the stabilization of mechanical single- and two-mode squeezed states has been recently achieved [13–16]. However, despite this success, the dissipative preparation of mechanical pure states is currently limited by the linear character of the evolution, which restricts the set of target states to Gaussian ones [17,18].

In order to prepare non-Gaussian—and especially nonclassical—states of motion, some source of nonlinearity is needed [19]. Early proposals for generating mechanical nonclassical states in optomechanical systems exploited the regime of single-photon strong coupling [20,21], which however is extremely weak in current experimental platforms. Conditional strategies have also been developed, e.g., based on photon-subtraction or pulsed interactions, which however suffer from being probabilistic and/or having a low efficiency [22–27]. In contrast, reservoir engineering guarantees the stable and unconditional preparation of the desired state.

In this paper we propose a dissipative scheme that exploits both the linear and the nonlinear (quadratic) optomechanical coupling between one cavity mode and one mechanical resonator to generate highly nonclassical states of motion of the mechanical element. In our scheme, the cavity provides a tunable reservoir whose properties are controlled by applying three coherent drives. A specific choice of their relative strengths and phases yields a class of bosonic steady states that admits a simple analytical expression. These states are (squeezed and displaced) finite superpositions of phonon number states with fixed parity and are parametrized by a non-negative integer n, which determines how many number states are superimposed. By selecting $n = 1$ we can stabilize a (squeezed displaced) single-phonon state, while for increasing n the state becomes a macroscopic quantum superposition similar to a Schrödinger cat state. Our scheme thus interpolates between the two prototypes of nonclassicality for bosonic systems: from single-excitation nonclassicality, revealed in the phase space by a single pronounced negativity of the Wigner function, to "interference fringes" typical of macroscopic superposition states. These features are shown to be robust against the effect of mechanical dissipation.

Contrary to existing proposals for the dissipative preparation of Schrödinger cat states that rely on a purely quadratic optomechanical coupling [28,29], our scheme does not require initialization to the ground state, given that the target state corresponds to a unique steady state. Our proposal also differs from that of Refs. [30,31] inasmuch as it does not require any anharmonicity of the potential. Finally, our protocol does not rely on the prohibitive single-photon strong coupling, which has been exploited to stabilize mechanical single-phonon states [32] and certain sub-Poissonian states [33].

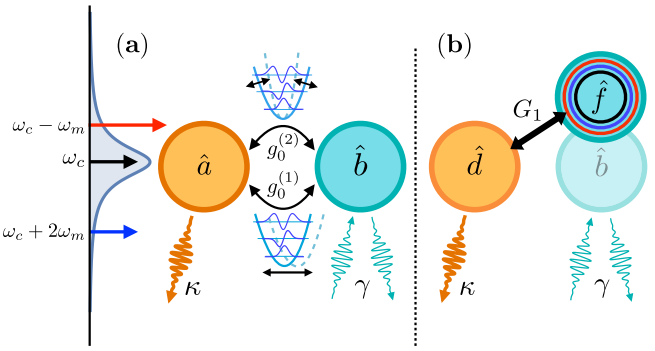

FIG. 1. (a) A cavity mode ($\hat{a}$) and a mechanical oscillator ($\hat{b}$) are coupled via a linear-and-quadratic optomechanical interaction with strength $g_0^{(1,2)}$ [Eq. (1)]. The cavity is driven with three lasers as shown on the left-hand side. (b) The cavity fluctuation $\hat{d}$ is coupled via a beam-splitter interaction (with strength G_1) to the operator $\hat{f}$, which is a nonlinear function of $\hat{b}$ [Eqs. (2) and (3)] and whose form is determined by the relative strengths and phases among the drives (symbolized by the circles). The prevailing cavity losses, which couple the system at a rate κ to an environment with zero thermal occupation, drive the oscillator toward the desired state [Eqs. (7) or (8)] while mechanical damping at a rate γ introduces imperfections (see Fig. 3).

II. MODEL

We consider a cavity mode whose frequency is parametrically coupled to the displacement and the displacement squared of a mechanical resonator. The Hamiltonian is given by (we set $\hbar = 1$ throughout)

$$\hat{H} = \omega_c \hat{a}^\dagger \hat{a} + \omega_m \hat{b}^\dagger \hat{b} - g_0^{(1)} \hat{a}^\dagger \hat{a} (\hat{b} + \hat{b}^\dagger) - g_0^{(2)} \hat{a}^\dagger \hat{a} (\hat{b} + \hat{b}^\dagger)^2, \tag{1}$$

where $\hat{a}$ ($\hat{b}$) describes the cavity (mechanical) mode with frequency ω_c (ω_m) and $g_0^{(1,2)}$ quantifies the single-photon coupling strengths [34]. We refer to the term in Eq. (1) proportional to the mechanical position (position squared) as the linear (quadratic) term; as sketched in Fig. 1(a), its action consists in the displacement (squeezing) of the mechanical mode conditioned on the number of cavity photons.

The cavity is driven with three lasers, one red-detuned by one mechanical frequency, one blue-detuned by twice the mechanical frequency, and one resonant, as schematically shown in Fig. 1(a). The effect of the drives is taken into account by the displacement transformation $\hat{a} = \sum_k \alpha_k e^{-i\omega_k t} + \hat{d}$, where α_k is the intracavity amplitude at each driving frequency ω_k and $\hat{d}$ is a quantum fluctuation. Moving to a frame rotating with the cavity and mechanical frequencies, we can write the displaced Hamiltonian as $\hat{H} = \hat{H}_{\rm RWA} + \hat{H}_{\rm CR}$, where $\hat{H}_{\rm RWA}$ contains the transitions resonantly enhanced by the drives while $\hat{H}_{\rm CR}$ collects the off-resonant terms. If we restrict ourselves to the limit $|G_{1,2,3}| \ll \omega_m$, $|RG_1| \ll \omega_m$, and $|R^{-1}G_{2,3}| \ll \omega_m$, where $R = g_0^{(2)}/g_0^{(1)}$, $G_1 = \alpha_1 g_0^{(1)}$, and $G_{2(3)} = \alpha_{2(3)} g_0^{(2)}$, we can neglect the counter-rotating terms and consider only the resonant contributions (cf. Appendix A)

$$\hat{H}_{\rm RWA} = G_1(\hat{d}^\dagger \hat{f} + \hat{d}\, \hat{f}^\dagger), \tag{2}$$

where we have introduced the operator

$$\hat{f} = \hat{b} + \frac{G_2}{G_1}\hat{b}^{\dagger 2} + \frac{G_3}{G_1}(\hat{b}\hat{b}^\dagger + \hat{b}^\dagger \hat{b}). \tag{3}$$

In the following we take the coefficients $G_{1,2,3}$ to to be real without loss of generality. Equation (2) describes a beam-splitter interaction between the cavity fluctuation and a nonlinear combination of the mechanical creation and annihilation operators, as shown in Fig. 1(b). The form of Eq. (3) stems from the joint presence of the linear and the quadratic coupling between one cavity mode and *one* mechanical oscillator; coupling to *different* cavity modes was recently considered to obtain a tunable optomechanical nonlinearity [35].

We also need to take into account the effect of dissipation. We start by including the dominant cavity losses, in which case the evolution of the joint density matrix $\hat{\varrho}$ reads

$$\dot{\hat{\varrho}} = -i[\hat{H}_{\rm RWA}, \hat{\varrho}] + \kappa\, \mathcal{D}_{\hat{d}}[\hat{\varrho}], \tag{4}$$

where $\mathcal{D}_{\hat{o}}[\hat{\varrho}] = \hat{o}\hat{\varrho}\hat{o}^\dagger - \frac{1}{2}(\hat{o}^\dagger \hat{o}\hat{\varrho} + \hat{\varrho}\hat{o}^\dagger \hat{o})$ is the standard dissipator. Provided that a stationary state exists, this is given by $\hat{\varrho}_{ss} = |\psi_{ss}\rangle\langle\psi_{ss}|$, with $|\psi_{ss}\rangle = |0\rangle \otimes |\varphi\rangle$ and where the mechanical state obeys the dark-state condition [36]

$$\hat{f}|\varphi\rangle = 0. \tag{5}$$

By varying the number, strength, and frequency of the drives, reservoir engineering with linear-and-quadratic coupling allows to stabilize a plethora of nonclassical states and manifolds thereof [37]. In the following we focus on a particularly relevant instance.

Family of steady states. We now introduce and characterize a family of states that are generated within the scheme presented above. If we assume

$$G_3 = -G_2 = \frac{G_1}{2\sqrt{2n+1}}, \tag{6}$$

where $n \in \mathbb{N}_0$ is a non-negative integer, the mechanical steady state $|\varphi\rangle \equiv |\varphi_n\rangle$ is described by the surprisingly simple wave function

$$\varphi_n(x) \propto e^{-\frac{X_n^2}{4}} H_n(X_n). \tag{7}$$

In the equation above, $\varphi_n(x) = \langle x|\varphi_n\rangle$ and $H_n(X_n)$ is the Hermite polynomial of argument $X_n = \sqrt{\frac{2}{3}}(x + \sqrt{4n+2})$.

This expression has been obtained by solving the differential equation associated with Eq. (5) (cf. Appendix D). The choice of the coupling strengths as in Eq. (6), and in particular the introduction of an integer parameter, are crucial to obtain such a simple expression. Nevertheless, we verified numerically that, for small deviations from these values, the steady state (now no longer pure) has near-unit fidelity with the target state described by Eq. (7), so that no fine-tuning issue arises.

The stationary wave function $\varphi_n(x)$ resembles that of a simple harmonic oscillator, but with two crucial differences: (i) the integer n appearing both in the order and in the argument of the Hermite polynomial and (ii) the presence of a factor 4 in the exponential. The latter, albeit seemingly innocuous, prevents $\varphi_n(x)$ from being recast into the standard harmonic oscillator form and, in fact, entails a superposition of harmonic oscillator wave functions. The corresponding

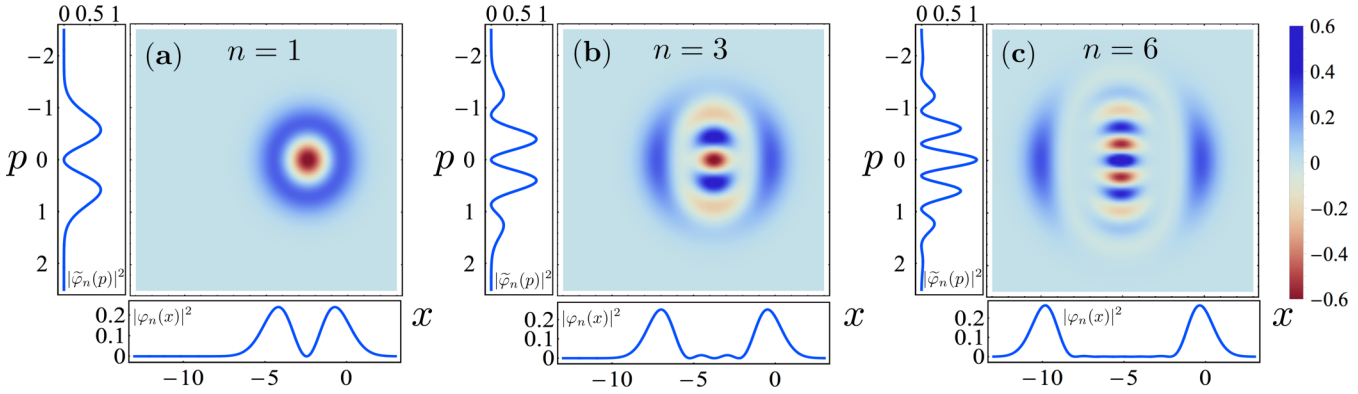

FIG. 2. Wigner function $W(x, p)$ of the state $|\varphi_n\rangle$ [Eq. (8)] for (a) $n = 1$, (b) $n = 3$, and (c) $n = 6$. The marginals of $W(x, p)$, which provide the position and momentum probability distribution, are also shown.

state is indeed a squeezed and displaced superposition of a finite number of Fock states (cf. Appendix D)

$$|\varphi_n\rangle \propto \hat{D}(\zeta_n)\hat{S}(r)\sum_{j=0}^{\lfloor \frac{n}{2} \rfloor} \frac{1}{2^{2j}\, j!\sqrt{(n-2j)!}}|n-2j\rangle, \quad (8)$$

where $\hat{S}(r)$ and $\hat{D}(\zeta_n)$ are the squeezing and displacement operators of argument $r = \ln\sqrt{3}$ and $\zeta_n = -\sqrt{2n+1}$, respectively, and $\lfloor y \rfloor$ yields the greatest integer smaller than or equal to y. Equation (8) provides the exact expression of an instance of a bosonic state and represents one of the main results of this work. Unlike coherent or squeezed states, for which the coefficients are found by writing the definition [analog of Eq. (5)] in the Fock basis and solving a recurrence relation, such an attempt here would fail. Instead, our approach of first obtaining the wave function by projecting the dark-state condition onto the position eigenstates and from that deriving a closed expression for the coefficients proves successful.

The state $|\varphi_n\rangle$ consists of two Gaussian unitary operations acting on a *finite* superposition of Fock states, which is responsible for its nonclassical nature. This finite seed contains at most n excitations, has a definite number parity, and can be in principle isolated by deterministically counter-squeezing and displacing the state. Theoretical proposals to achieve probabilistically the truncation of photon number superpositions have been put forward for linear optical devices [38,39]. In contrast, here a finite superposition can be obtained unconditionally, without exploiting entanglement and for a massive system. These states may thus be useful for quantum information processing as a robust choice for qubit encoding [40], similarly to what has already been proposed for Schrödinger cat states [41,42].

In Fig. 2 we show the Wigner function $W(x, p) = \frac{1}{\pi}\int \mathrm{d}y\, e^{-2ipy}\varphi_n(x+y)\varphi_n^*(x-y)$ of $|\varphi_n\rangle$ for different values of n. The transition from a single pronounced negativity [Fig. 2(a)] to phase-space "ripples" [Figs. 2(b) and 2(c)] is apparent. It is useful to compare our solution to the family of Schrödinger cat states $|\mathcal{C}_\alpha^\pm\rangle \propto |\alpha\rangle \pm |-\alpha\rangle$ [43], for which optomechanical realizations exploiting reservoir engineering have been proposed [28,29,31]. Contrary to the case of an odd cat state $|\mathcal{C}_\alpha^-\rangle$, which in the limit of small amplitude *approximates* a single-phonon state—the so-called kitten state [44]—the state $|\varphi_1\rangle = \hat{D}(\zeta_1)\hat{S}(r)|1\rangle$ is *exactly* a (squeezed and displaced) single-phonon state. On the other hand, for large n the state $|\varphi_n\rangle$ approaches a Schrödinger cat, yet the two never fully overlap (even asymptotically unit fidelity is not attained), so that Eq. (8) embodies a similar but distinct instance of a macroscopic quantum superposition (cf. Appendix E).

III. RATE OF APPROACHING THE STEADY STATE AND EFFECTS OF MECHANICAL DISSIPATION

We now address how the unavoidable presence of mechanical damping affects the properties of the target state. For simplicity, we focus on the fast cavity limit $\kappa \gg G_k$, where adiabatic elimination of the cavity field leads to an effective master equation for the reduced mechanical density matrix (see Refs. [45,46] or cf. Appendix B for explicit derivation)

$$\dot{\hat{\varrho}}^{(m)} = \gamma\mathcal{C}\,\mathcal{D}_f\,[\hat{\varrho}^{(m)}] + \gamma(\bar{n}+1)\mathcal{D}_b[\hat{\varrho}^{(m)}] + \gamma\bar{n}\mathcal{D}_{b^\dagger}[\hat{\varrho}^{(m)}], \quad (9)$$

where $\mathcal{C} = 4G_1^2/(\gamma\kappa)$ defines the optomechanical cooperativity. The first term on the right-hand side describes dissipation induced by the modified jump operator

$$\hat{f} = \hat{b} - \frac{1}{2\sqrt{2n+1}}[\hat{b}^{\dagger 2} - (\hat{b}\hat{b}^\dagger + \hat{b}^\dagger\hat{b})], \quad (10)$$

which makes manifest the role played by the cavity in providing an engineered environment for the mechanical degree of freedom. In Eq. (9) we also added thermal decoherence to a mechanical bath at a rate γ and with $\bar{n}$ thermal occupancy.

Let us first consider the limit of no mechanical damping. In this case Eq. (9) describes a purely dissipative dynamics, however relative to a jump operator that is *neither linear nor bosonic*; complete information about the dynamics can be uncovered by studying the spectrum of $\mathcal{D}_f$. In the infinite-time limit the state $\hat{\varrho}_{ss}^{(m)} = \lim_{t\to\infty}\hat{\varrho}^{(m)}$ satisfies $\mathcal{D}_f[\hat{\varrho}_{ss}^{(m)}] = 0$ and is nondegenerate. We can conclude that our protocol is both deterministic and independent of the choice of the initial state, allowing in principle to start from any given state, e.g., a thermal one. This must be contrasted with dissipative preparation of mechanical cat states [28,29], for which the steady state has a double degeneracy and consequently initialization to a

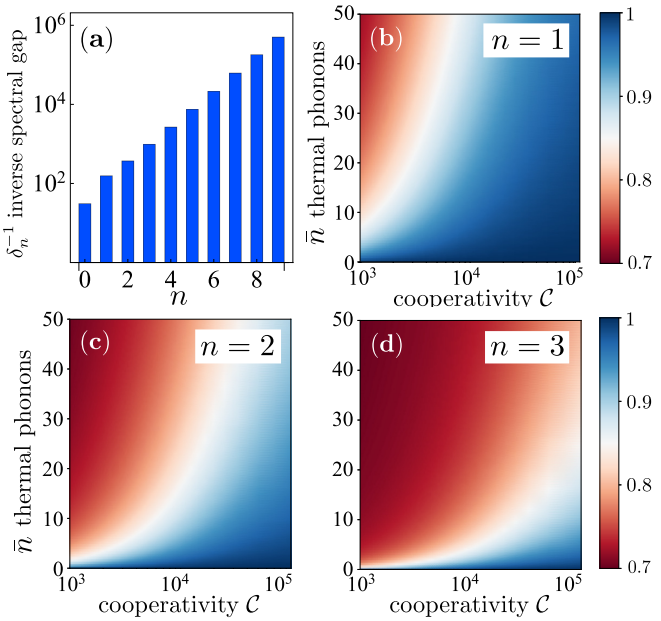

FIG. 3. (a) Plot of the inverse spectral gap δ_n^{-1} of the dissipator $\mathcal{D}_f$ with jump operator as in Eq. (10) for different n, in units of $(\gamma\mathcal{C})^{-1}$. $\delta_n/(\gamma\mathcal{C}) = -\mathrm{Re}\,\lambda_n$, with λ_n the smallest nonzero eigenvalue. (b)–(d) Fidelity between the target state Eq. (8) and the steady state in the presence of mechanical damping as a function of $\bar{n}$ and γ (parametrized by the cooperativity $\mathcal{C}$) for (b) $n = 1$, (c) $n = 2$, and (d) $n = 3$. We set $G_1 = 0.05\kappa$.

state of definite parity—typically the ground state—is needed. The presence of a linear part in $\hat{f}$ breaks the discrete parity symmetry associated with the quadratic terms and makes the system more robust to losses [47]. We also stress that our method enables the preparation of macroscopic superposition states of chosen parity, while reservoir engineering of odd cat states is highly impractical, as it requires to initialize the state to a pure odd-parity state, e.g., in $|1\rangle$.

The analysis of the spectrum also provides information about the timescale required to reach the steady state. The slowest decaying term is associated with the eigenvalue λ_n that has the smallest nonzero real part, which in turn defines the spectral gap $\delta_n/(\gamma\mathcal{C}) = -\mathrm{Re}\,\lambda_n$. The time needed to approach the steady state (with a fixed fidelity) scales as $\tau_n \sim \delta_n^{-1}$. As pointed out, when n increases, the state $|\varphi_n\rangle$ realizes a macroscopic superposition. On the other hand, from Eq. (10) we see that for increasing n the nonlinear terms are suppressed with respect to the cooling part: the optimal strategy to prepare a large quantum superposition is therefore to minimally perturb—in the way prescribed by Eq. (10)—a standard cooling process, which is recovered by setting $G_2 = G_3 = 0$ in Eq. (3). However, we find that the spectral gap is exponentially suppressed with respect to n and therefore τ_n grows exponentially, as shown in Fig. 3(a). It also represents the main limiting factor of our protocol for the generation of macroscopic quantum states when thermal decoherence is taken into account.

We finally introduce a nonzero coupling with the bath. Figures 3(b)–3(d) show the mismatch, quantified by the fidelity [48], between the actual steady state and the target state in Eq. (8). As expected, mechanical dissipation is responsible for a decrease of the purity and states with greater n are more susceptible to thermal decoherence. Nevertheless, we see that regions of near-unit fidelity are present even for considerable thermal occupancy. Moreover, even if the fidelity is no longer close to one, we show that the steady state retains nonclassical features and is always non-Gaussian (in the range of parameters explored, see Appendix F).

IV. EXPERIMENTAL IMPLEMENTATION

To implement our idea, we consider a three-mode optomechanical system made of a pair of two-dimensional (2D) photonic crystal cavities in a double-slotted configuration separated by a central mechanical beam [49,50]. When the beam is equidistant from the two slabs, an enhanced quadratic optomechanical coupling is obtained [51]. On the other hand, a shift in the beam's position, which can be controlled via electrostatic actuation, determines a tunable coupling that has both a linear and a quadratic component (cf. Appendix C). To estimate the single-photon couplings, we consider the following realistic parameters from Ref. [50]: photon tunneling rate between left and right cavity $J/2\pi = 0.1$ GHz, bare frequency pull parameter $g_L = -g_R = 100$ GHz/nm, zero-point amplitude of the nanobeam $x_{\mathrm{zpf}} = 10$ fm, and application of a bias voltage of a few tenth of a millivolt (that guarantees a displacement $x_0 < 0.1$ pm). These parameters yield $g_0^{(2)} \approx 5$ kHz and $g_0^{(1)} \approx 70$ kHz, and hence a ratio $R \approx 0.07$, for which the rotating-wave approximation (RWA) in Eq. (2) is justified (see Appendix A for details). The central beam supports several acoustic modes ranging from a few megahertz to a few gigahertz, with modes of frequency $\omega_m > 300$ MHz lying deep in the resolved-sideband regime. Photonic crystal cavities allow for large intracavity photon capacities $n_c > 10^4$, which give couplings $G_{1,2,3}$ in the 10–100 MHz range. The reasonable choice of the parameters $Q_m = 10^6$, $\omega_m/2\pi = 400$ MHz, $\kappa/2\pi = 50$ MHz, $n_c = 10^4$, and $g_0^{(1)} = 70$ kHz gives a multiphoton cooperativity $\mathcal{C} \approx 10^4$, which can be easily increased by one order of magnitude by considering higher mechanical Q and/or higher couplings. This would allow for the stabilization of our target state with high fidelity also without initialization in the ground state.

Once the target state $\hat{\varrho}_{ss}^{(m)}$ has been prepared, a cavity mode (different from the one providing the engineered reservoir) can be employed for the readout. Tomographic schemes via quantum nondemolition (QND) coupling have been proposed both in the good [52,53] and bad cavity limits [54–57] and can be directly apply here. A less demanding task would be the certification of the nonclassicality of the state, which can be accomplished with a single homodynelike measurement [56]. In photonic crystal architecture, it may be especially convenient to exploit the optomechanical interaction with one of the two cavity supermodes for the preparation and the other for the readout.

V. CONCLUSIONS

The linear and the quadratic couplings achievable in optomechanical systems have so far been addressed separately. We showed that the joint presence of both terms enables engineering of unique nonclassical features in the

state of a mechanical resonator. Our proposal achieves the unconditional preparation of states of a macroscopic object featuring a nonpositive Wigner function.

ACKNOWLEDGMENTS

We thank M. Sillanpää and T. K. Paraïso for helpful discussions. This work was supported by the European Union's Horizon 2020 research and innovation programme under Grant No. 732894 (FET Proactive HOT). A.N. acknowledges a University Research Fellowship from the Royal Society and additional support from the Winton Programme for the Physics of Sustainability. D.M. acknowledges the Coordinator Support funds from Queen's University Belfast. O.H. and M.P. acknowledge support from the SFI-DfE Investigator programme (Grant No. 15/IA/2864). O.H., A.F., and M.P. are supported by the EU Horizon2020 Collaborative Project TEQ (Grant No. 766900). A.F. and O.H. acknowledge funding from the EPSRC project EP/P00282X/1. M.P. thanks COST Action CA15220 QTSpace for partial support.

M.B. and O.H. contributed equally to this work.

APPENDIX A: DERIVATION OF THE HAMILTONIAN AND THE EFFECT OF COUNTER-ROTATING TERMS

We consider an optomechanical system where the frequency of a cavity mode parametrically couples to the displacement and the displacement squared of a mechanical resonator [34]. The Hamiltonian is given by ($\hbar = 1$)

$$\hat{H} = \hat{H}_0 + \hat{H}_{\rm int} + \hat{H}_{\rm drive}, \tag{A1}$$

where we set

$$\hat{H}_0 = \omega_c \hat{a}^\dagger \hat{a} + \omega_m \hat{b}^\dagger \hat{b}, \tag{A2a}$$

$$\hat{H}_{\rm int} = -g_0^{(1)} \hat{a}^\dagger \hat{a}(\hat{b} + \hat{b}^\dagger) - g_0^{(2)} \hat{a}^\dagger \hat{a}(\hat{b} + \hat{b}^\dagger)^2, \tag{A2b}$$

$$\hat{H}_{\rm drive} = \mathcal{E}(t)\hat{a}^\dagger + \mathcal{E}^*(t)\hat{a}. \tag{A2c}$$

The first of these expressions, Eq. (A2a), contains the free oscillating terms, where $\hat{a}$ ($\hat{b}$) describes the cavity (mechanical) mode with frequency ω_c (ω_m). The second, Eq. (A2b), describes the linear and the quadratic optomechanical interaction with single-photon coupling strength $g_0^{(k)} = -x_{\rm zpf}^k 2^{1-k} \partial_x^k \omega_c(\hat{x})|_{x=0}$, $k = 1, 2$, $\hat{x}$ being the (dimensionless) mechanical displacement and $x_{\rm zpf}$ the zero-point fluctuation. The last expression, Eq. (A2c), includes a coherent drive of the cavity with multiple tones of frequency ω_k and amplitude ϵ_k, namely, $\mathcal{E}(t) = \sum_k \epsilon_k e^{-i\omega_k t}$.

The cavity is in contact with an effective zero-temperature reservoir provided by the extracavity modes, while the mechanical oscillator is in contact with a bath of inverse temperature β that induces $\bar{n} = (e^{\beta\omega_m} - 1)^{-1}$ average thermal excitations [43,45]. We assume for both processes the Markovian limit, that translates into the following expressions for the correlation functions of the optical ($\hat{a}_{\rm in}$) and mechanical ($\hat{b}_{\rm in}$) input noise operator:

$$\langle \hat{a}_{\rm in}(t)\hat{a}_{\rm in}^\dagger(t')\rangle = \delta(t - t'), \quad \langle \hat{a}_{\rm in}^\dagger(t)\hat{a}_{\rm in}(t')\rangle = 0, \tag{A3a}$$

$$\langle \hat{b}_{\rm in}(t)\hat{b}_{\rm in}^\dagger(t')\rangle = (\bar{n} + 1)\delta(t - t'),$$

$$\langle \hat{b}_{\rm in}^\dagger(t)\hat{b}_{\rm in}(t')\rangle = \bar{n}\,\delta(t - t'). \tag{A3b}$$

The Heisenberg-Langevin equations for the system are thus given by

$$\dot{\hat{a}} = -i\big[\omega_c - g_0^{(1)}(\hat{b} + \hat{b}^\dagger) - g_0^{(2)}(\hat{b} + \hat{b}^\dagger)^2\big]\hat{a} - \frac{\kappa}{2}\hat{a} - i\mathcal{E} + \sqrt{\kappa}\hat{a}_{\rm in}, \tag{A4a}$$

$$\dot{\hat{b}} = -i\omega_m \hat{b} + i\big[g_0^{(1)} + 2ig_0^{(2)}(\hat{b} + \hat{b}^\dagger)\big]\hat{a}^\dagger a - \frac{\gamma}{2}\hat{b} + \sqrt{\gamma}\hat{b}_{\rm in}, \tag{A4b}$$

where κ and γ are the optical and the mechanical damping rates.

We then separate the contributions to the dynamics into mean field and fluctuations, i.e., $\hat{a}(t) = \alpha(t) + \hat{d}(t)$. After a transient, we expect the cavity field to follow the modulation of the drive, i.e., $\alpha(t) = \sum_k \alpha_k e^{-i\omega_k t}$. Driving multiple frequencies leads to amplitude modulation of the intracavity field, which in turn translates into an oscillating force acting on the mechanical element. This fact can be taken into account by decomposing also the mechanical mode into mean field and fluctuations, $\hat{b}(t) = \beta(t) + \hat{h}(t)$. Furthermore, if we restrict ourselves to the limit $g_0^{(j)}\alpha_k\alpha_l \ll \omega_m$, $j = 1, 2$, the mean fields attain a stationary value, which we refer to as $\alpha_{k,s}$, β_s. The steady amplitudes take the following expressions:

$$\alpha_{k,s} = \frac{-i\epsilon_k}{\frac{\kappa}{2} - i\big[\Delta_k + g_0^{(1)}(\beta_s + \beta_s^*) + g_0^{(2)}(\beta_s + \beta_s^*)^2\big]}, \tag{A5a}$$

$$\beta_s = \frac{g_0^{(1)} \sum_k |\alpha_{k,s}|^2 \big(\omega_m + i\frac{\gamma}{2}\big)}{\big(\frac{\gamma}{2}\big)^2 + \omega_m\big(\omega_m - 4g_0^{(2)} \sum_k |\alpha_{k,s}|^2\big)}, \tag{A5b}$$

where we set $\Delta_k = \omega_k - \omega_c$. We see that position and position-squared couplings lead to a shift of the equilibrium mechanical position and to a modified detuning. However, these effects are small and can be safely neglected; therefore, we set $\beta_s \approx 0$ and $\alpha_{k,s} = \frac{-i\epsilon_k}{\kappa/2 - i\Delta_k}$ in what follows.

Moving to an interaction picture with respect to $\hat{H}_0$ the Hamiltonian is transformed into

$$\hat{H} = -\sum_k (\alpha_k \hat{d}^\dagger e^{-i\Delta_k t} + \alpha_k^* \hat{d} e^{i\Delta_k t}) \times \big[g_0^{(1)}(\hat{b}e^{-i\omega_m t} + \hat{b}^\dagger e^{i\omega_m t}) + g_0^{(2)}(\hat{b}e^{-i\omega_m t} + \hat{b}^\dagger e^{i\omega_m t})^2\big]. \tag{A6}$$

We now consider the following choice for the drives,

$$\Delta_1 = -\omega_m, \quad \Delta_2 = 2\omega_m, \quad \Delta_3 = 0, \tag{A7}$$

which correspond to driving the first red mechanical sideband, the second blue sideband, and on the cavity resonance. This choice is to be understood *a posteriori*, as a suitable modification of a cavity cooling scheme that selects the nonlinear terms necessary to prepare the desired state. Indeed, for particular values of the strength and phase of the second and third drives with respect to the cooling beam, this setup cools the mechanical mode toward a nonclassical state of motion. The application of the drives displayed in Eq. (A7) makes the

following processes in the Hamiltonian Eq. (A6) resonant:

$$\hat{H}_{\rm RWA} = G_1(\hat{d}^\dagger \hat{f} + \hat{d}\,\hat{f}^\dagger), \tag{A8}$$

where

$$\hat{f} = \hat{b} + \frac{G_2}{G_1}\hat{b}^{\dagger 2} + \frac{G_3}{G_1}\{\hat{b}, \hat{b}^\dagger\}, \tag{A9}$$

and we set $G_1 = \alpha_1 g_0^{(1)}$, $G_{2(3)} = \alpha_{2(3)} g_0^{(2)}$, and $\{\cdot,\cdot\}$ is the anticommutator. The resonant contributions in Eq. (A8) describe a beam-splitter interaction between the fluctuation of the cavity field $\hat{d}$ and the nonlinear combination of mechanical creation and annihilation operators $\hat{f}$.

The counter-rotating terms $\hat{H}_{\rm CR} = \hat{H} - \hat{H}_{\rm RWA}$ are

$$\begin{aligned}\hat{H}_{\rm CR} = \hat{d}^\dagger \big\{ & e^{-i\omega_m t}\big(\alpha_2 g_0^{(1)}\hat{b}^\dagger + \alpha_3 g_0^{(1)}\hat{b} + \alpha_1 g_0^{(2)}\hat{b}^2\big) \\ & + e^{+i\omega_m t}\big(\alpha_3 g_0^{(1)}\hat{b}^\dagger + \alpha_1 g_0^{(2)}\{\hat{b}, \hat{b}^\dagger\}\big) \\ & + e^{-2i\omega_m t}\big(\alpha_2 g_0^{(2)}\{\hat{b}, \hat{b}^\dagger\} + \alpha_3 g_0^{(2)}\hat{b}^2\big) \\ & + e^{+2i\omega_m t}\big(\alpha_1 g_0^{(1)}\hat{b}^\dagger + \alpha_3 g_0^{(2)}\hat{b}^{\dagger 2}\big) \\ & + e^{-3i\omega_m t}\alpha_2 g_0^{(1)}\hat{b} + e^{+3i\omega_m t}\alpha_1 g_0^{(2)}\hat{b}^{\dagger 2} \\ & + e^{-4i\omega_m t}\alpha_2 g_0^{(2)}\hat{b}^2\big\} + \text{H.c.}\end{aligned} \tag{A10}$$

We rewrite the oscillating terms as $\hat{H}_{\rm CR} = \sum_{k=1}^{4} e^{i\omega_m k t}\hat{H}_{\rm CR}^{(k)} + \text{H.c.}$, with

$$\begin{aligned}\hat{H}_{\rm CR}^{(1)} &= R^{-1}G_2\hat{d}\hat{b} + R^{-1}(G_3\hat{d}^\dagger + G_3\hat{d})\hat{b}^\dagger + RG_1\hat{d}\hat{b}^{\dagger 2} \\ &\quad + RG_1\hat{d}^\dagger\{\hat{b}, \hat{b}^\dagger\},\end{aligned} \tag{A11a}$$

$$\hat{H}_{\rm CR}^{(2)} = G_1\hat{d}^\dagger\hat{b}^\dagger + (G_3\hat{d}^\dagger + G_3\hat{d})\hat{b}^{\dagger 2} + G_2\hat{d}\{\hat{b}, \hat{b}^\dagger\}, \tag{A11b}$$

$$\hat{H}_{\rm CR}^{(3)} = R^{-1}G_2\hat{d}\hat{b}^\dagger + RG_1\hat{d}^\dagger\hat{b}^{\dagger 2}, \tag{A11c}$$

$$\hat{H}_{\rm CR}^{(4)} = G_2\hat{d}\hat{b}^{\dagger 2}, \tag{A11d}$$

where we introduced the ratio $R = g_0^{(2)}/g_0^{(1)}$ between the quadratic and the linear single-photon coupling strength. From this explicit form it is apparent that a necessary condition for the RWA to be valid is that

$$\big|G_{1,2,3}\big| \ll \omega_m, \quad |RG_1| \ll \omega_m, \quad \text{and} \quad \big|R^{-1}G_{2,3}\big| \ll \omega_m. \tag{A12}$$

We can verify the validity of the RWA by integrating numerically the time-dependent master equation

$$\dot{\hat{\varrho}} = -i[\hat{H}_{\rm RWA} + \hat{H}_{\rm CR}, \hat{\varrho}] + \kappa\,\mathcal{D}_d[\hat{\varrho}] \tag{A13}$$

and comparing its long-time average with the steady state of the same master equation when omitting the counter-rotating terms $\hat{H}_{\rm CR}$. In the following we choose the driving amplitudes such that

$$G_3 = -G_2 = \frac{G_1}{2\sqrt{2n+1}}, \tag{A14}$$

where n is a non-negative integer. In Fig. 4 we show the fidelity between the two steady states of the master equation (A13), with and without $\hat{H}_{\rm CR}$, as a function of the ratio R for different values of $n = 0, 1, 2, 3$ and the parameters $\kappa = 0.001\omega_m$, $G_1 = 0.01\kappa$. We can see that there exist ranges of values of R, within the region identified by the conditions in Eq. (A12), for which the rotating-wave approximation is fully justified (for the parameters under consideration). The range of values R for which the counter-rotating terms can be neglected depends on n, and the fidelity develops a double-peak structure that shrinks for increasing n; this behavior can be understood from the fact that conditions (A12) depend on both the ratio R and its inverse. However, there is always a window of values R that achieves near-unit fidelity.

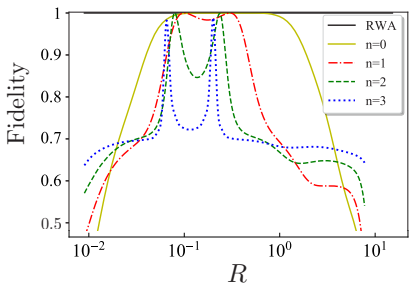

FIG. 4. Fidelity between the long-time average of the full master equation (A13) and the target state (8) as a function of the ratio $R = g_0^{(2)}/g_0^{(1)}$ between single-photon quadratic and linear coupling. Parameters are $\kappa = 0.001\omega_m$, $G_1 = 0.05\kappa$. The horizontal black line corresponds to taking the rotating-wave approximation; the solid yellow, dot-dashed red, dashed green, and dotted blue curves are for $n = 0, 1, 2, 3$, respectively.

APPENDIX B: DERIVATION OF THE EFFECTIVE MASTER EQUATION

In the main text we used an effective master equation for the mechanical degrees of freedom only, where the cavity field was adiabatically eliminated. Here we give a derivation of the effective master equation for a generic system consisting of a damped cavity mode coupled to an arbitrary function of the mechanical operators. The master equation describing the dynamics of the joint density operator is

$$\dot{\hat{\varrho}} = -i[\hat{H}, \hat{\varrho}] + \kappa\left(\hat{a}\hat{\varrho}\hat{a}^\dagger - \frac{1}{2}\hat{a}^\dagger\hat{a}\hat{\varrho} - \frac{1}{2}\hat{\varrho}\hat{a}^\dagger\hat{a}\right), \tag{B1}$$

where $\hat{H} = G(\hat{a}^\dagger\hat{f} + \hat{a}\,\hat{f}^\dagger)$, $\hat{a}$ is the cavity mode annihilation operator, κ is the cavity damping rate, and $\hat{f}$ a function of $\hat{b}$ and $\hat{b}^\dagger$.

We assume that there are two time scales in the system: a fast dynamics for the cavity and a slow one for the mechanical oscillator; this assumption translates into $G \ll \kappa$. To eliminate the cavity variables we use the recipe for adiabatic elimination developed in Ref. [58]: Master equation (B1) can be put in the form

$$\dot{\hat{\varrho}} = \mathcal{L}_0\hat{\varrho} + G\mathcal{L}_1\hat{\varrho}, \tag{B2}$$

where $\mathcal{L}_0\hat{\varrho} \equiv \kappa(\hat{a}\hat{\varrho}\hat{a}^\dagger - \frac{1}{2}\hat{a}^\dagger\hat{a}\hat{\varrho} - \frac{1}{2}\hat{\varrho}\hat{a}^\dagger\hat{a})$ and $\mathcal{L}_1\hat{\varrho} \equiv -i[\hat{H}_1, \hat{\varrho}]$, with $\hat{H}_1 \equiv \hat{H}/G$. Then we treat the second term of Eq. (B2) as a perturbation since we assumed that $G \ll \kappa$. We write the effective master equation for the mechanical oscillator in the form

$$\dot{\hat{\varrho}}_b = \mathcal{L}_b\hat{\varrho}_b, \tag{B3}$$

where $\hat{\varrho}_b$ is the density operator describing the mechanical state, and $\mathcal{L}_b$ is a Lindbladian. The latter is expressed as a power series in the perturbation parameter G:

$$\mathcal{L}_b\hat{\varrho}_b = \sum_{n\geqslant 1} G^n \mathcal{L}_{b,n}\hat{\varrho}_b \,. \tag{B4}$$

Up to second order in perturbation theory, $\mathcal{L}_{b,1}$ and $\mathcal{L}_{b,2}$ are given by the expressions [58]

$$\mathcal{L}_{b,1}\hat{\varrho}_b = -i[\hat{H}_b, \hat{\varrho}_b] \,, \tag{B5}$$

$$\mathcal{L}_{b,2}\hat{\varrho}_b = \sum_\ell \left(\hat{B}_\ell \hat{\varrho}_b \hat{B}_\ell^\dagger - \frac{1}{2}\{\hat{B}_\ell^\dagger \hat{B}_\ell, \hat{\varrho}_b\} \right), \tag{B6}$$

where $\hat{H}_b = \hat{S}^\dagger \hat{H}_1 \hat{S}$ and $\hat{B}_\ell = 2\hat{S}^\dagger \hat{M}_\ell \hat{L}(\hat{L}^\dagger\hat{L})^{-1}\hat{H}_1\hat{S}$ with $\hat{L} \equiv \sqrt{\kappa}\hat{a}$ and $\hat{S}$ and $\hat{M}_\ell$ are the operators defined as follows: in the absence of perturbation ($G = 0$) the system evolves toward the steady state $|0\rangle_a\langle 0| \otimes \mathrm{Tr}_a[\hat{\varrho}(0)]$. The set of all steady states (when the initial state $\hat{\varrho}(0)$ varies) has the support $|0\rangle_a \otimes |\ell\rangle_b$ ($\ell = 0, 1, \ldots$). The operator $\hat{S}$ is defined as $\hat{S} = \sum_\ell (|0\rangle_a \otimes |\ell\rangle_b)_b\langle\ell|$ and $\hat{M}_\ell$ are obtained from the relation $|0\rangle_a\langle 0| \otimes \mathrm{Tr}_a[\hat{\varrho}(0)] = \sum_\ell \hat{M}_\ell \hat{\varrho}(0) \hat{M}_\ell^\dagger$ with the condition $\sum_\ell \hat{M}_\ell^\dagger \hat{M}_\ell = \mathbb{1}$ (the identity operator in the Hilbert space of the system). It is straightforward to obtain $\hat{M}_\ell = |0\rangle_a\langle\ell| \otimes \mathbb{1}_b$ ($\mathbb{1}_b$ denotes the identity operator in the Hilbert space of the mechanical oscillator). With these expressions we find $\hat{H}_b = 0$ and $\hat{B}_\ell = \frac{2}{\sqrt{\kappa}}\,\delta_{\ell,0}\hat{f}$, so that the effective master equation reads

$$\dot{\hat{\varrho}}_b = \frac{4G^2}{\kappa}\left(\hat{f}\hat{\varrho}_b\hat{f}^\dagger - \frac{1}{2}\{\hat{f}^\dagger\hat{f}, \hat{\varrho}_b\} \right). \tag{B7}$$

This is the reduced master equation (9) upon the identification $G \equiv G_1$, $\hat{a} \equiv \hat{d}$, $\hat{\varrho}_b \equiv \hat{\varrho}^{(m)}$, and $\hat{f}$ as in Eq. (10).

APPENDIX C: IMPLEMENTATION

The system we consider for implementing our scheme consists of a pair of two-dimensional photonic crystal cavities, obtained by patterning two thin silicon films, separated by a central suspended mechanical beam, also realized with a photonic crystal with a single row of holes (nanobeam). The two cavities host localized degenerate optical modes $\hat{a}_L$ and $\hat{a}_R$ of the same frequency ω and are coupled at a rate J via photon hopping across the central mechanical beam $\hat{b}$ of frequency ω_m. A sketch of this multimode setup is given in Fig. 5. Details about the experimental realization of such a device can be found in Ref. [49], while Ref. [50] provides an in-depth study of the optical and acoustic modes accessible in this multimode structure and their optomechanical properties. The Hamiltonian of the three-mode optomechanical system is given by

$$\hat{H}_{\mathrm{tot}} = \hat{H}_0 + \hat{H}_{\mathrm{hop}} + \hat{H}_{\mathrm{int}}, \tag{C1}$$

$$\hat{H}_0 = \omega(\hat{a}_L^\dagger\hat{a}_L + \hat{a}_R^\dagger\hat{a}_R) + \omega_m\hat{b}^\dagger\hat{b}, \tag{C2}$$

$$\hat{H}_{\mathrm{hop}} = J(\hat{a}_L^\dagger\hat{a}_R + \hat{a}_R^\dagger\hat{a}_L), \tag{C3}$$

$$\hat{H}_{\mathrm{int}} = x_{\mathrm{zpf}}(\hat{b} + \hat{b}^\dagger)(g_L\hat{a}_L^\dagger\hat{a}_L + g_R\hat{a}_R^\dagger\hat{a}_R). \tag{C4}$$

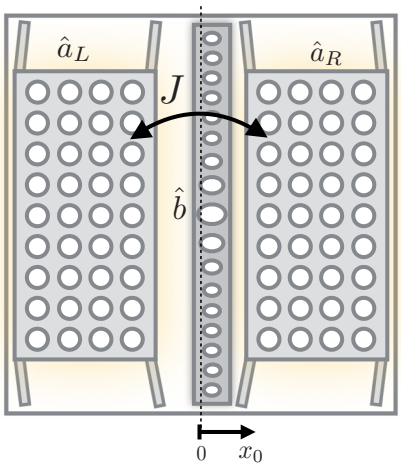

FIG. 5. Sketch of an optomechanical crystal implementation of a tunable linear-and-quadratic coupling. Due to photons hopping through the central nanobeam (mode $\hat{b}$), localized photonic modes $\hat{a}_{L,R}$ hybridize into supermodes delocalized over the two photonic cavities. The supermodes are optomechanically coupled to the nanobeam displacement and displacement squared. When the beam is equidistant from the two slabs ($x_0 = 0$), a purely quadratic optomechanical coupling is realized, while a controlled offset of the nanobeam displacement $x_0 \neq 0$ enables arbitrary linear-and-quadratic couplings.

Due to the tunneling, the localized optical modes hybridize into supermodes. The Hamiltonian written in the supermode basis $\hat{a}_\pm = (\hat{a}_L \pm \hat{a}_R)/\sqrt{2}$ can be diagonalized by assuming a quasistatic approximation of the mechanical motion, resulting in eigenfrequencies $\omega_\pm = \omega_\pm(\hat{x})$ that are given by [51]

$$\omega_\pm(\hat{x}) = \omega + g_\pm\hat{x} \pm \sqrt{J^2 + g_{+-}^2\hat{x}^2}, \tag{C5}$$

where $\hat{x} = x_{\mathrm{zpf}}(\hat{b} + \hat{b}^\dagger)$ and

$$g_+ = g_- = \frac{g_L + g_R}{2} \quad \text{and} \quad g_{+-} = \frac{g_L - g_R}{2} \tag{C6}$$

are referred to as linear self-mode coupling and linear cross-mode coupling, respectively. For the geometry we consider one has $g_L = -g_R$, so that by expanding Eq. (C5) around the position equidistant from the two slabs ($x_0 = 0$) one is left with a purely quadratic interaction with enhanced optomechanical coupling $g_0^{(2)} = \frac{g_{+-}^2}{2J}x_{\mathrm{zpf}}^2$. The enhancement follows from the fact that J can be made arbitrarily small. On the other hand, when the central beam position is not equidistant from the two crystal cavities, i.e., the two air slots are not of the same width, the expansion of the supermode frequency around $x_0 \neq 0$ leads to both a linear and a quadratic term. The expressions read [50]

$$g_\pm(x_0) \approx \frac{g_L + g_R}{2} \pm \frac{g_L - g_R}{2}\frac{Z}{\sqrt{Z^2+1}}, \tag{C7}$$

$$g_{+-}(x_0) \approx \frac{g_L - g_R}{2}\frac{1}{\sqrt{Z^2+1}}, \tag{C8}$$

where $Z = \frac{(g_L - g_R)}{2J} x_0$, which entail single-photon optomechanical coupling of the form

$$g_0^{(1)} = g_{\pm}(x_0)\, x_{\mathrm{zpf}}, \tag{C9}$$

$$g_0^{(2)} = \frac{g_{+-}^2(x_0)}{2J} \frac{1}{(Z^2+1)^{3/2}} x_{\mathrm{zpf}}^2. \tag{C10}$$

The separation of the slots with respect to the central beam can be fine-tuned via electrostatic actuation, which provides extremely refined control over the ratio $R = g_0^{(2)}/g_0^{(1)}$. To estimate the single-photon couplings we consider the following values, taken from the finite-element simulation of Ref. [50]: $J/2\pi = 0.1$ GHz, $x_{\mathrm{zpf}} = 10$ fm, application of a bias voltage of a few tenths of a millivolt that guarantees a displacement $x_0 < 0.1$ pm (Ref. [59] reports a measured tunability of 0.05 nm/V^2 in a similar double-slotted photonic crystal cavity), and $g_L = -g_R = 100$ GHz/nm. Plugging these parameters in Eqs. (C9) and (C10) yields $g_0^{(2)} \approx 5$ kHz and $g_0^{(1)} \approx 70$ kHz, and thus $R \approx 0.07$, for which the RWA is an excellent approximation for several values of n considered in Fig. 4. In general, depending on the specific target state $|\varphi_n\rangle$ to be stabilized, the ratio R needs to be tuned to the required value(s).

The central beam hosts several acoustic modes, both flexural mechanical resonances and localized "breathing" modes, ranging from a few megahertz to a few gigahertz. A large cavity quality factor of $Q \approx 4 \times 10^6$ at the telecom wavelength $\lambda = 1550$ nm places mechanical modes of frequency $\omega_m > 300$ MHz deep in the resolved-sideband regime. For the specific deign of Ref. [50], finite-element simulations give for such high-frequency modes $x_{\mathrm{zpf}} \approx 3$ fm, which however is not much smaller than the one we have assumed for the estimate of the bare optomechanical couplings. Photonic crystal cavities allow for large intracavity photon capacities $n_c > 10^4$, which gives the multiphoton optomechanical couplings $G_{1,2,3}$ in the 10–100 MHz range. Assuming a mechanical quality factor $Q_m = 10^6$, a mechanical frequency $\omega_m/2\pi = 400$ MHz, a cavity decay rate $\kappa/2\pi = 50$ MHz, intracavity photon number $n_c = 10^4$, and $g_0^{(1)} = 70$ kHz gives a multiphoton cooperativity $\mathcal{C} \approx 10^4$. This would allow for the stabilization of our target state with high fidelity also without initialization in the ground state (see Fig. 3). To give a reference, at the dilution refrigerator temperature of 15 mK the thermal occupation of a mode $\omega_m/2\pi = 400$ MHz (1 GHz) is $\bar{n} = 0.39$ (0.04), which increases to $\bar{n} = 52$ (20) at 1 K. Larger values of the cooperativity can be obtained by considering higher mechanical quality factors and/or higher couplings.

APPENDIX D: DERIVATION OF THE STEADY-STATE SOLUTION

In this section we derive the analytic expressions for the wave function, Eq. (7), and from that obtain the Fock-state decomposition presented in Eq. (8). We also discuss how a finite accuracy in tuning the coefficients to the values prescribed by Eq. (A14) affects the target state.

1. Wave function

The dark-state condition, Eq. (5), relative to the combination of mechanical creation and annihilation operators, Eq. (A9), can be equivalently expressed as the following differential equation for the system wave function $\varphi(x) = \langle x|\varphi\rangle$:

$$\left(\tfrac{G_2}{2} - G_3\right)\varphi''(x) + \left(\tfrac{G_1}{\sqrt{2}} - G_2 x\right)\varphi'(x) + \left[-\tfrac{G_2}{2} + \tfrac{G_1}{\sqrt{2}} x + \left(\tfrac{G_2}{2} + G_3\right)x^2\right]\varphi(x) = 0. \tag{D1}$$

This is a second-order linear, homogeneous equation, whose only square integrable solution (for suitable values of the coefficients $G_{1,2,3}$) comes in the form of a Hermite function, i.e., a Hermite polynomial times a Gaussian function. The explicit expression is rather involved, and hence not reported. We can simplify it by demanding that the order of the Hermite polynomial, which is expressed as a combination of $G_{1,2,3}$, reduces to a non-negative integer value $n \in \mathbb{N}_0$. This constraint can be expressed, e.g., as $G_2 = G_2(n, G_1, G_3)$. Moreover, upon direct inspection of the solution one can see that the expression greatly simplifies by choosing G_3 and G_2 equal and *opposite*. This choice fixes the form of the coefficients, whose magnitude is given by $|G_2| = |G_3| = \frac{G_1}{2\sqrt{2n+1}}$ and in the following we consider the case $G_3 > 0$, as shown in Eq. (A14). As a result, the wave function acquires a universal character, depending only on the parameter n, and takes the remarkably simple form

$$\varphi_n(x) = \mathcal{N}_n e^{-\frac{X_n^2}{4}} H_n(X_n), \tag{D2}$$

where we introduced $X_n = \sqrt{\frac{2}{3}}(x + \sqrt{4n+2})$ and $\mathcal{N}_n = (3\pi)^{-\frac{1}{4}} \sqrt{\frac{n!}{(2n)!\, {}_2F_1(-n,-n;-n+\frac{1}{2};-\frac{1}{2})}}$ is the normalization constant, ${}_2F_1(a,b;c;z)$ being the Gaussian hypergeometric function of argument z. We stress that values of the ratio between the quadratic terms G_3 and G_2 different from that in Eq. (A14) also lead to legitimate wave functions (for some the solution of Eq. (5) no longer describes a pure state), whose properties, however, may be very different from those of $\varphi_n(x)$ and whose nonclassical features are generally suppressed.

Figure 6 shows plots of the wave function, Eq. (D2), for different values of n (left-hand panel), together with the corresponding probability density function (right-hand panel). We notice how the wave functions relative to an even or odd integer n have distinct parity, as for the case of a simple harmonic oscillator. However, compared to the latter, the central oscillations of $\varphi_n(x)$ are progressively suppressed for increasing values of n and at the same time the probability density develops a distinct bimodal character; this feature witnesses the transition to a Schrödinger-cat-like state for increasing n.

Unlike the quantum harmonic oscillator, where integer values labeling the solutions follow from the quantization of energy levels and the wave functions form an orthonormal set, in our case there are no fundamental mechanisms forbidding noninteger values—these being determined by the choice of the drives—and different $\varphi_n(x)$ are not orthogonal. The similarities between the two wave functions are due to the fact that

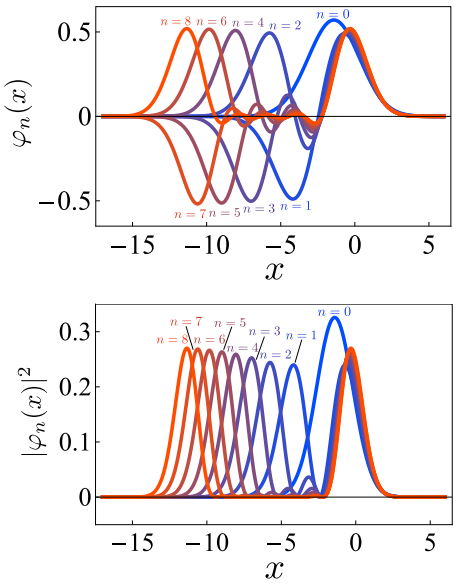

FIG. 6. Wave function $\varphi_n(x)$ (top) and corresponding probability density (bottom) from $n = 0$ (blue) to $n = 8$ (orange).

the dark-state condition, Eq. (D1), resembles the Hermite differential equation encountered in the stationary Schrödinger equation for a harmonic potential. However, since the ratio between the coherent drives can only be tuned up to a finite precision, it is important to verify that the target state is well behaved with respect to imperfections. We then proceed to include small deviations from the optimal couplings shown in Eq. (A14),

$$G_2 = G_1\left(\frac{-1}{2\sqrt{2n+1}} + \delta_1\right),$$
$$G_3 = G_1\left(\frac{1}{2\sqrt{2n+1}} + \delta_2\right), \tag{D3}$$

and check the deviation of the steady state from the ideal one. Figure 7 confirms that the state is robust with respect to imprecisions in the strength of the drives.

2. Fock-state representation

We now derive the explicit decomposition of the state $|\varphi_n\rangle$ in the Fock basis. To achieve this goal, we start from the expression of the wave function, Eq. (D2), and exploit the rescaling property of the Hermite polynomials that, for any $\gamma \in \mathbb{R}$, is given by

$$H_n(\gamma x) = \sum_{j=0}^{\lfloor \frac{n}{2} \rfloor} \gamma^{n-2j}(\gamma^2-1)^j \binom{n}{2j} \frac{(2j)!}{j!} H_{n-2j}(x). \tag{D4}$$

The wave function is thus rewritten as

$$\varphi_n(x) = \mathcal{N}_n e^{-\frac{1}{2}(\frac{X_n}{\sqrt{2}})^2} H_n\left(\sqrt{2}\,\frac{X_n}{\sqrt{2}}\right), \tag{D5a}$$
$$= \mathcal{N}_n \sum_{j=0}^{\lfloor \frac{n}{2} \rfloor} 2^{\frac{n}{2}-j} \binom{n}{2j} \frac{(2j)!}{j!} e^{-\frac{1}{2}(\frac{X_n}{\sqrt{2}})^2} H_{n-2j}\left(\frac{X_n}{\sqrt{2}}\right), \tag{D5b}$$

where $\lfloor y \rfloor$ is the floor function of argument y. We hence see that the wave function, Eq. (D2), is in fact a superposition of $\lfloor \frac{n}{2} \rfloor + 1$ harmonic oscillator wave functions of argument $X_n/\sqrt{2}$. Moreover, each of these is easily identified with the wave function of a squeezed displaced number state. Indeed, one finds

$$\langle x|\hat{D}(\zeta)\hat{S}(r)|n\rangle = \frac{1}{\pi^{\frac{1}{4}}\sqrt{2^n n! e^r}} e^{-\frac{1}{2}(\frac{x+\sqrt{2}\zeta}{e^r})^2} H_n\left(\frac{x+\sqrt{2}\zeta}{e^r}\right), \tag{D6}$$

where $\hat{D}(\zeta)$ and $\hat{S}(r)$ are displacement and squeezing transformations that, for real parameters, reduce to $\hat{D}(\zeta) = e^{-i\sqrt{2}\zeta\hat{p}}$ and $\hat{S}(r) = e^{-i\frac{r}{2}(\hat{x}\hat{p}+\hat{p}\hat{x})}$. Therefore, combining Eqs. (D5b) and (D6) we can write

$$\varphi_n(x) = \pi^{\frac{1}{4}}\mathcal{N}_n \sum_{j=0}^{\lfloor \frac{n}{2} \rfloor} 2^{\frac{n}{2}-j} \binom{n}{2j} \frac{(2j)!}{j!} \sqrt{2^{n-2j}(n-2j)!e^r}$$
$$\times \langle x|\hat{D}(\zeta_n)\hat{S}(r)|n-2j\rangle, \tag{D7}$$

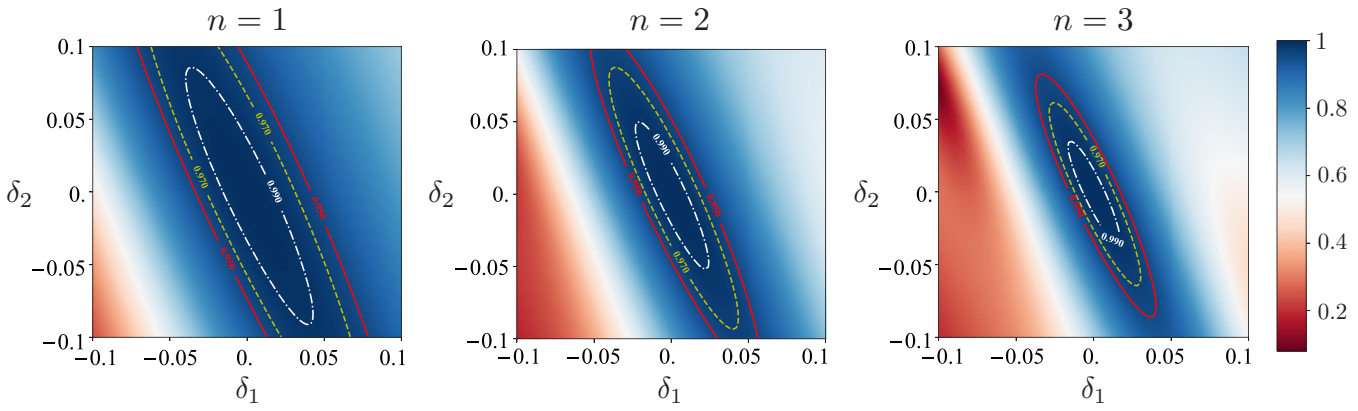

FIG. 7. Fidelity between the target state, Eq. (8), and the steady state obtained with perturbed couplings, Eq. (D3). The fidelity is plotted against relative errors δ_1 (horizontal axis) and δ_2 (vertical axis) for $n = 1$ (left), $n = 2$ (center), and $n = 3$ (right).

where we set

$$r = \frac{1}{2}\ln 3, \quad \text{and} \quad \zeta_n = -\sqrt{2n+1}. \tag{D8}$$

From Eq. (D7) we can finally read the expression for the state in the Fock basis,

$$|\varphi_n\rangle = \mathcal{M}_n \hat{D}(\zeta_n)\hat{S}(r)\sum_{j=0}^{\lfloor \frac{n}{2} \rfloor} \frac{1}{2^{2j} j!\sqrt{(n-2j)!}}|n-2j\rangle, \tag{D9}$$

where now the normalization factor reads $\mathcal{M}_n = \sqrt{\frac{n!}{{}_2F_1(\frac{1-n}{2}, \frac{-n}{2}; 1; \frac{1}{4})}}$. It is also clear that reversing the sign between G_2 and G_3 amounts to a change of displacement direction.

APPENDIX E: COMPARISON WITH SCHRÖDINGER CAT STATES

We are now interested in comparing the target state of our protocol with a Schrödinger cat state, which is a well-known benchmark for macroscopic quantum superposition states. We consider cat states of the following form:

$$|\mathcal{C}_\alpha^\pm\rangle = \mathcal{N}_\alpha^\pm(|\alpha\rangle \pm |-\alpha\rangle), \tag{E1}$$

where the normalization factor is given by $\mathcal{N}_\alpha^\pm = [2(1 \pm e^{-2|\alpha|^2})]^{-\frac{1}{2}}$ and the plus (minus) sign selects an even (odd) cat state, namely, a superposition of only even (odd) number states. For a better comparison we also consider the target state $|\varphi_n\rangle$ without the squeezing and the displacement term, thus focusing on the finite superposition. The fidelity between the two states is computed as $\mathcal{F}^\pm(\alpha, n) = |\langle \mathcal{C}_\alpha^\pm | \widetilde{\varphi}_n\rangle|$, where

$$|\widetilde{\varphi}_n\rangle = \mathcal{M}_n \sum_{j=0}^{\lfloor \frac{n}{2} \rfloor} \frac{1}{2^{2j} j!\sqrt{(n-2j)!}}|n-2j\rangle. \tag{E2}$$

Given that both states have definite parity, the only nonzero overlaps are between an even/odd cat state and an even/odd superposition of Fock states, and their expressions read

$$\mathcal{F}^+(\alpha, 2n) = \frac{\mathcal{M}_{2n}}{\sqrt{\cosh|\alpha|^2}}\left|\sum_{j=0}^{n} \frac{(\alpha^*)^{2(n-j)}}{2^{2j} j!(2(n-j))!}\right|, \tag{E3a}$$

$$\mathcal{F}^-(\alpha, 2n+1) = \frac{\mathcal{M}_{2n+1}}{\sqrt{\sinh|\alpha|^2}}\left|\sum_{j=0}^{n} \frac{(\alpha^*)^{2(n-j)+1}}{2^{2j} j!(2(n-j)+1)!}\right|. \tag{E3b}$$

In Fig. 8 we show the maximum fidelity $\mathcal{F}^\pm_{\max} = \mathcal{F}^\pm(\alpha_{\max}, n)$, optimized over α, between an even (odd) cat state and even (odd) finite superposition of Fock states. The fidelity always lies within the range $\mathcal{F}^\pm_{\max} \approx 0.9-1$, providing further evidence that our state is indeed a macroscopic quantum superposition; larger values of n correspond to larger superposition states, as also witnessed by the increasing amplitude of the "closest" cat state, shown in the right-hand panel. However, by increasing n, the fidelity does not approach 1 and in fact saturates to a value $\mathcal{F}^\pm_{\max} \approx 0.92$, thus confirming that

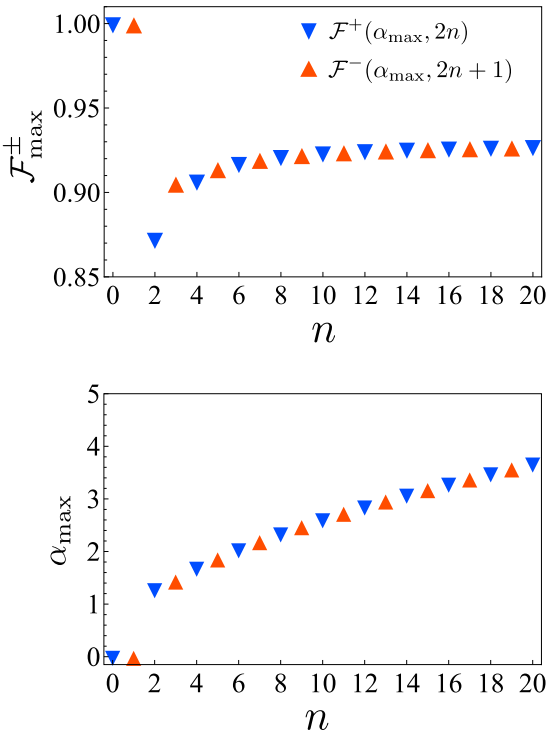

FIG. 8. Top: Maximum fidelity between even (odd) Schrödinger cat states and even (odd) finite superpositions for different integers n. Bottom: Values of the amplitude of the cat state yielding optimal fidelity for each n.

$|\mathcal{C}_\alpha^\pm\rangle$ and $|\varphi_n\rangle$ provide similar but always *distinct* instances of macroscopic superposition states.

APPENDIX F: EFFECTS OF THE MECHANICAL DAMPING ON THE NONCLASSICALITY

We now address how the nonclassical features of the target state, Eq. (8), are affected by the presence of mechanical damping. To this aim, we consider the volume of the negative portion of the Wigner function, i.e., $\nu^{(-)} = \int_{\mathbb{R}^2} dxdpW(x,p)^{(-)}$, where $W(x,p)^{(-)} = \frac{1}{2}\{|W(x,p)| - W(x,p)\}$, which is known to provide an indicator of the nonclassicality of the state [60]. In the limit $\gamma \to 0$ the Wigner function $W(x,p) = \frac{1}{\pi}\int dx\, e^{-2ipy}\varphi_n(x+y)\varphi_n^*(x-y)$ can be expressed analytically from Eq. (D2), although for the general state $|\varphi_n\rangle$ its form is quite cumbersome and hence not reported. For $\gamma \neq 0$ we numerically obtain $\hat{\varrho}_{ss}^{(m)}$ as the solution of $\mathcal{D}_f[\hat{\varrho}_{ss}^{(m)}] = 0$ and compute its Wigner function. Notice that, by definition, the quantity $\nu^{(-)}$ vanishes for nonclassical yet *Gaussian* states such as a squeezed vacuum state. A plot of $\nu^{(-)}$ as a function of $\bar{n}$ and γ (parametrized by the cooperativity $\mathcal{C}$) is shown in Fig. 9, for different values of n. As expected, the negative volume is suppressed by the presence of mechanical dissipation and reduction of $\nu^{(-)}$ is more pronounced for increasing n. However, the steady state is nonclassical for a large range of values, even when it no longer has near-unit fidelity with the target pure state Eq. (8) (cf. Fig. 3). In particular, the state is non-Gaussian for all the values shown.

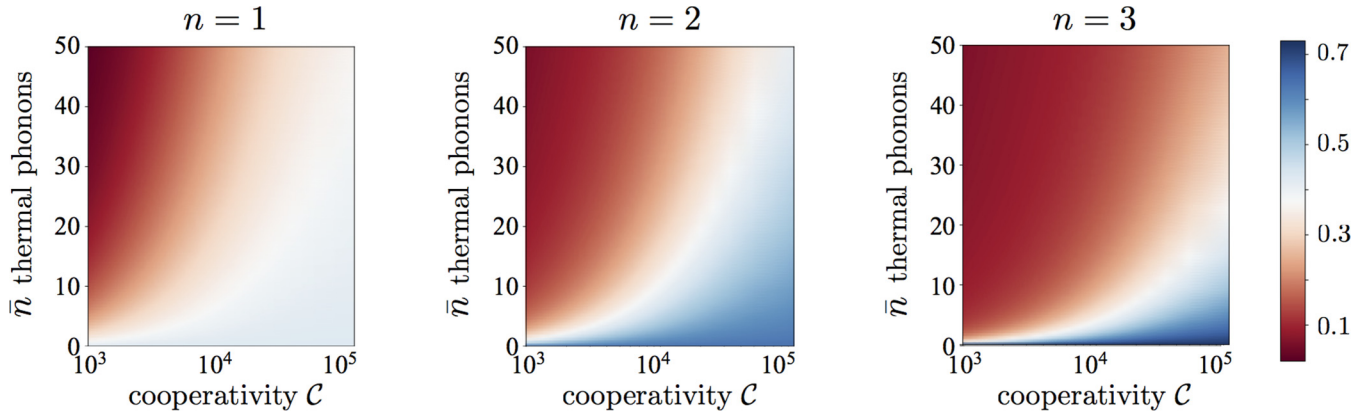

FIG. 9. Negative volume of the Wigner function [of the steady state of Eq. (9)] in the presence of mechanical damping as a function of $\bar{n}$ and γ (parametrized by the cooperativity $\mathcal{C}$), for $n = 1$ (left), $n = 2$ (center), and $n = 3$ (right). $G_1 = 0.05\kappa$.

[1] J. F. Poyatos, J. I. Cirac, and P. Zoller, Quantum Reservoir Engineering with Laser Cooled Trapped Ions, Phys. Rev. Lett. **77**, 4728 (1996).

[2] H. Krauter, C. A. Muschik, K. Jensen, W. Wasilewski, J. M. Petersen, J. I. Cirac, and E. S. Polzik, Entanglement Generated by Dissipation and Steady State Entanglement of Two Macroscopic Objects, Phys. Rev. Lett. **107**, 080503 (2011).

[3] J. T. Barreiro, M. Müller, P. Schindler, D. Nigg, T. Monz, M. Chwalla, M. Hennrich, C. F. Roos, P. Zoller, and R. Blatt, An open-system quantum simulator with trapped ions, Nature (London) **470**, 486 (2011).

[4] Y. Lin, J. P. Gaebler, F. Reiter, T. R. Tan, R. Bowler, A. S. Sorensen, D. Leibfried, and D. J. Wineland, Dissipative production of a maximally entangled steady state of two quantum bits, Nature (London) **504**, 415 (2013).

[5] D. Kienzler, H.-Y. Lo, B. Keitch, L. de Clercq, F. Leupold, F. Lindenfelser, M. Marinelli, V. Negnevitsky, and J. P. Home, Quantum harmonic oscillator state synthesis by reservoir engineering, Science **347**, 53 (2015).

[6] S. Shankar, M. Hatridge, Z. Leghtas, K. M. Sliwa, A. Narla, U. Vool, S. M. Girvin, L. Frunzio, M. Mirrahimi, and M. H. Devoret, Autonomously stabilized entanglement between two superconducting quantum bits, Nature (London) **504**, 419 (2013).

[7] Z. Leghtas, S. Touzard, I. M. Pop, A. Kou, B. Vlastakis, A. Petrenko, K. M. Sliwa, A. Narla, S. Shankar, M. J. Hatridge, M. Reagor, L. Frunzio, R. J. Schoelkopf, M. Mirrahimi, and M. H. Devoret, Confining the state of light to a quantum manifold by engineered two-photon loss, Science **347**, 853 (2015).

[8] A. Kronwald, F. Marquardt, and A. A. Clerk, Arbitrarily large steady-state bosonic squeezing via dissipation, Phys. Rev. A **88**, 063833 (2013).

[9] Y.-D. Wang and A. A. Clerk, Reservoir-Engineered Entanglement in Optomechanical Systems, Phys. Rev. Lett. **110**, 253601 (2013).

[10] M. J. Woolley and A. A. Clerk, Two-mode squeezed states in cavity optomechanics via engineering of a single reservoir, Phys. Rev. A **89**, 063805 (2014).

[11] J. Li, I. Moaddel Haghighi, N. Malossi, S. Zippilli, and D. Vitali1, Generation and detection of large and robust entanglement between two different mechanical resonators in cavity optomechanics, New J. Phys. **17**, 103037 (2015).

[12] O. Houhou, H. Aissaoui, and A. Ferraro, Generation of cluster states in optomechanical quantum systems, Phys. Rev. A **92**, 063843 (2015).

[13] E. E. Wollman, C. U. Lei, A. J. Weinstein, J. Suh, A. Kronwald, F. Marquardt, A. A. Clerk, and K. C. Schwab, Quantum squeezing of motion in a mechanical resonator, Science **349**, 952 (2015).

[14] J.-M. Pirkkalainen, E. Damskägg, M. Brandt, F. Massel, and M. A. Sillanpää, Squeezing of Quantum Noise of Motion in a Micromechanical Resonator, Phys. Rev. Lett. **115**, 243601 (2015).

[15] F. Lecocq, J. B. Clark, R. W. Simmonds, J. Aumentado, and J. D. Teufel, Quantum Nondemolition Measurement of a Nonclassical State of a Massive Object, Phys. Rev. X **5**, 041037 (2015).

[16] C. F. Ockeloen-Korppi, E. Damskägg, J.-M. Pirkkalainen, M. Asjad, A. A. Clerk, F. Massel, M. J. Woolley, and M. A. Sillanpää, Entangled massive mechanical oscillators, Nature (London) **556**, 478 (2018).

[17] C. Weedbrook, S. Pirandola, R. Garcìa-Patròn, N. J. Cerf, T. C. Ralph, J. H. Shapiro, and S. Lloyd, Gaussian quantum information, Rev. Mod. Phys. **84**, 621 (2012).

[18] A. Ferraro, S. Olivares, and M. G. A. Paris, *Gaussian States in Quantum Information* (Bibliopolis, Napoli, 2005).

[19] Since our focus is on the preparation of non-Gaussian states, we take to be "nonclassical" a state that exhibits negativity in the Wigner function. A more stringent notion of nonclassicality, based on the negativity and/or singularity of the Glauber-Sudarshan P function, can be considered, which, however, includes Gaussian states, e.g., squeezed vacuum.

[20] S. Bose, K. Jacobs, and P. L. Knight, Preparation of nonclassical states in cavities with a moving mirror, Phys. Rev. A **56**, 4175 (1997).

[21] W. Marshall, C. Simon, R. Penrose, and D. Bouwmeester, Towards Quantum Superpositions of a Mirror, Phys. Rev. Lett. **91**, 130401 (2003).

[22] M. Paternostro, Engineering Nonclassicality in a Mechanical System Through Photon Subtraction, Phys. Rev. Lett. **106**, 183601 (2011).

[23] O. Romero-Isart, A. C. Pflanzer, F. Blaser, R. Kaltenbaek, N. Kiesel, M. Aspelmeyer, and J. I. Cirac, Large Quantum Superpositions and Interference of Massive Nanometer-Sized Objects, Phys. Rev. Lett. **107**, 020405 (2011).

[24] M. M. Khan, M. J. Akram, M. Paternostro, and F. Saif, Engineering single-phonon number states of a mechanical oscillator via photon subtraction, Phys. Rev. A **94**, 063830 (2016).

[25] U. B. Hoff, J. Kollath-Bönig, J. S. Neergaard-Nielsen, and U. L. Andersen, Measurement-Induced Macroscopic Superposition States in Cavity Optomechanics, Phys. Rev. Lett. **117**, 143601 (2016).

[26] M. R. Vanner, Selective Linear or Quadratic Optomechanical Coupling via Measurement, Phys. Rev. X **1**, 021011 (2011).

[27] G. A. Brawley, M. R. Vanner, P. E. Larsen, S. Schmid, A. Boisen, and W. P. Bowen, Nonlinear optomechanical measurement of mechanical motion, Nat. Commun. **7**, 10988 (2016).

[28] H. Tan, F. Bariani, G. Li, and P. Meystre, Generation of macroscopic quantum superpositions of optomechanical oscillators by dissipation, Phys. Rev. A **88**, 023817 (2013).

[29] M. Asjad and D. Vitali, Reservoir engineering of a mechanical resonator: Generating a macroscopic superposition state and monitoring its decoherence, J. Phys. B **47**, 045502 (2014).

[30] S. Rips, M. Kiffner, I. Wilson-Rae, and M. J. Hartmann, Steady-state negative Wigner functions of nonlinear nanomechanical oscillators, New J. Phys. **14**, 023042 (2012).

[31] M. Abdi, P. Degenfeld-Schonburg, M. Sameti, C. Navarrete-Benlloch, and M. J. Hartmann, Dissipative Optomechanical Preparation of Macroscopic Quantum Superposition States, Phys. Rev. Lett. **116**, 233604 (2016).

[32] K. Børkje, Scheme for steady-state preparation of a harmonic oscillator in the first excited state, Phys. Rev. A **90**, 023806 (2014).

[33] G.-F. Xu and C. K. Law, Dark states of a moving mirror in the single-photon strong-coupling regime, Phys. Rev. A **87**, 053849 (2013).

[34] M. Aspelmeyer, T. J. Kippenberg, and F. Marquardt, Cavity optomechanics, Rev. Mod. Phys. **86**, 1391 (2014).

[35] G.-L. Zhu, Xin-You Lü, Liang-Liang Wan, Tai-Shuang Yin, Qian Bin, and Ying Wu, Controllable nonlinearity in a dual-coupling optomechanical system under a weak-coupling regime, Phys. Rev. A **97**, 033830 (2018).

[36] B. Kraus, H. P. Büchler, S. Diehl, A. Kantian, A. Micheli, and P. Zoller, Preparation of entangled states by quantum Markov processes, Phys. Rev. A **78**, 042307 (2008).

[37] M. Brunelli and O. Houhou, Linear-and-quadratic reservoir engineering of non-Gaussian states, arXiv:1809.05266.

[38] D. T. Pegg, L. S. Phillips, and S. M. Barnett, Optical State Truncation by Projection Synthesis, Phys. Rev. Lett. **81**, 1604 (1998).

[39] S. K. Özdemir, A. Miranowicz, M. Koashi, and N. Imoto, Quantum-scissors device for optical state truncation: A proposal for practical realization, Phys. Rev. A **64**, 063818 (2001).

[40] D. Gottesman, A. Kitaev, and J. Preskill, Encoding a qubit in an oscillator, Phys. Rev. A **64**, 012310 (2001).

[41] H. Jeong and T. C. Ralph, in *Quantum Information with Continuous Variables of Atoms and Light* (Imperial College Press, London, 2007), pp. 159–177.

[42] M. Mirrahimi, Z. Leghtas, V. V. Albert, S. Touzard, R. J. Schoelkopf, Liang Jiang, and M. H. Devoret, Dynamically protected cat-qubits: A new paradigm for universal quantum computation, New J. Phys. **16**, 045014 (2014).

[43] D. F. Walls and G. J. Milburn, *Quantum Optics* (Springer, Berlin, 2008).

[44] A. Ourjoumtsev, R. Tualle-Brouri, J. Laurat, and P. Grangier, Generating optical Schrödinger kittens for quantum information processing, Science **312**, 83 (2006).

[45] C. W. Gardiner and P. Zoller, *Quantum Noise* (Springer, Berlin, 2000).

[46] H. Wiseman and G. J. Milburn, Quantum theory of field-quadrature measurements, Phys. Rev. A **47**, 642 (1993).

[47] V. V. Albert and L. Jiang, Symmetries and conserved quantities in Lindblad master equations, Phys. Rev. A **89**, 022118 (2014).

[48] A. Uhlmann, The transition probability in the state space of a *-algebra, Rep. Math. Phys. **9**, 273 (1976).

[49] T. K. Paraïso, M. Kalaee, L. Zang, H. Pfeifer, F. Marquardt, and O. Painter, Position-Squared Coupling in a Tunable Photonic Crystal Optomechanical Cavity, Phys. Rev. X **5**, 041024 (2015).

[50] M. Kalaee, T. K. Paraïso, H. Pfeifer, and O. Painter, Design of a quasi-2D photonic crystal optomechanical cavity with tunable, large x^2-coupling, Opt. Express **24**, 21308 (2016).

[51] M. Ludwig, A. H. Safavi-Naeini, O. Painter, and F. Marquardt, Enhanced Quantum Nonlinearities in a Two-Mode Optomechanical System, Phys. Rev. Lett. **109**, 063601 (2012).

[52] A. A. Clerk, F. Marquardt, and K. Jacobs, Back-action evasion and squeezing of a mechanical resonator using a cavity detector, New J. Phys. **10**, 095010 (2008).

[53] D. W. Moore, T. Tufarelli, M. Paternostro, and A. Ferraro, Quantum state reconstruction of an oscillator network in an optomechanical setting, Phys. Rev. A **94**, 053811 (2016).

[54] M. R. Vanner, I. Pikovski, G. D. Cole, M. S. Kim, C. Brukner, K. Hammerer, G. J. Milburn, and M. Aspelmeyer, Pulsed quantum optomechanics, Proc. Natl. Acad. Sci. USA **108**, 16182 (2011).

[55] M. R. Vanner, J. Hofer, G. D. Cole, and M. Aspelmeyer, Cooling-by-measurement and mechanical state tomography via pulsed optomechanics, Nat. Commun. **4**, 2295 (2013).

[56] F. Shahandeh and M. Ringbauer, Optomechanical state reconstruction and nonclassicality verification beyond the resolved-sideband regime, arXiv:1709.01135.

[57] M. R. Vanner, I. Pikovski, and M. S. Kim, Towards optomechanical quantum state reconstruction of mechanical motion, Ann. Phys. **527**, 15 (2015).

[58] R. Azouit, A. Sarlette, and P. Rouchon, *2016 IEEE 55th Conference on Decision and Control* (IEEE, New York, 2016), pp. 4559–4565.

[59] M. Winger, T. D. Blasius, T. P. Mayer Alegre, A. H. Safavi-Naeini, S. Meenehan, J. Cohen, S. Stobbe, and O. Painter, A chip-scale integrated cavity-electro-optomechanics platform, Opt. Express **19**, 24905 (2011).

[60] A. Kenfack and K. Zyczkowski, Negativity of the Wigner function as an indicator of non-classicality, J. Opt. B **6**, 396 (2004).